Analyst

Microbial respiration and natural attenuation of benzene contaminated soils investigated by cavity enhanced Raman multi-gas spectroscopy

Journal:	*Analyst*
Manuscript ID:	AN-ART-01-2015-000091.R1
Article Type:	Paper
Date Submitted by the Author:	21-Feb-2015
Complete List of Authors:	Jochum, Tobias; Leibniz Institute of Photonic Technology, Michalzik, Beate; Friedrich Schiller University Jena, Bachmann, Anne; Leibniz Institute of Photonic Technology, Popp, Jürgen; Leibniz Institute of Photonic Technology, Frosch, Torsten; Friedrich Schiller University, Physical Chemistry; Institute of Photonic Technologies,

Journal Name

RSCPublishing

ARTICLE

Microbial respiration and natural attenuation of benzene contaminated soils investigated by cavity enhanced Raman multi-gas spectroscopy

Cite this: DOI: 10.1039/x0xx00000x

Received 00th January 2012,
Accepted 00th January 2012

DOI: 10.1039/x0xx00000x

www.rsc.org/

Tobias Jochum[a], Beate Michalzik[b], Anne Bachmann[a], Jürgen Popp[acd], and Torsten Frosch[ac*]

Soil and groundwater contamination with benzene can cause serious environmental damages. However, many soil microorganisms are capable to adapt and are known to strongly control the fate of organic contamination. Innovative cavity enhanced Raman multi-gas spectroscopy (CERS) was applied to investigate the short-term response of the soil micro-flora to sudden surface contamination with benzene regarding the temporal variations of gas products and their exchange rates with the adjacent atmosphere. ^{13}C-labeled benzene was spiked on a silty-loamy soil column in order to track and separate the changes in heterotrophic soil respiration - involving $^{12}CO_2$ and O_2 - from the natural attenuation process of benzene degradation to ultimately form $^{13}CO_2$. The respiratory quotient (RQ) decreased from value 0.98 to 0.46 directly after the spiking and increased again within 33 hours to a value of 0.72. This coincided with maximum $^{13}CO_2$ concentration rates (0.63 µmol m^{-2} s^{-1}), indicating highest benzene degradation at 33 hours after the spiking event. The diffusion of benzene in the headspace and the biodegradation into $^{13}CO_2$ were simultaneously monitored and 12 days after the benzene spiking no measurable degradation was detected anymore. The RQ finally returned to a value of 0.96 demonstrating the reestablished aerobic respiration.

Introduction

Monitored natural attenuation refers "to the reliance on natural attenuation processes (within the context of a carefully controlled and monitored site cleanup approach) to achieve site-specific remediation objectives within a time frame that is reasonable compared to that offered by other more active methods", according to U.S. EPA[1]. Other terms associated with natural attenuation include for instance "intrinsic remediation or bioremediation", "passive bioremediation", "natural recovery", and "natural assimilation". Those natural processes are used to reduce the concentration and amount of pollutants in contaminated soils and groundwater, encompassing microbial biodegradation, dispersion, dilution, volatilization and contaminant sorption onto soil solids. As low cost means compared to thermal and other physico-chemical techniques, natural attenuation has become of widespread interest[2-4]. However, to test the effectiveness of natural attenuation processes and underlying mechanisms under varying physico-chemical conditions and indigenous microflora, the contamination needs to be carefully monitored through the process[5, 6]. Benzene, as an important component of gasoline and widespread precursor in chemical industry, is a major organic pollutant in soils and groundwater. Due to its toxicity as carcinogenic and teratogenic agent, a detailed characterization of possible benzene decontamination by microbial remediation processes is required in order to estimate the soil quality and the effectiveness of decontamination. One approach for elucidating the metabolic pathways of this degradation is the quantification of the gas exchange rates between the soil and the atmosphere.

The most common used sensing technique for environmental gas analysis is lab-based gas chromatography[7], usually coupled to mass spectrometry[8] or flame ionization detection[9]. Although highly sensitive and selective, this technique is slow, sample consumptive and limited in terms of mobility. Infrared (IR) absorption spectroscopy methods[10-12] feature very high sensitivities for molecules with permanent dipole moment, such as carbon dioxide or methane, down to the ppm and ppb range[13]. However, IR based techniques are not suitable for the detection of crucial homonuclear atmospheric gases like N_2 or O_2. Especially quantifying dioxygen consumption rates is fundamental for calculating the respiratory quotient (RQ) and thus deducing microbial activity[14]. Raman spectroscopy is an emerging technique[15-18], based on molecular

vibrations[19-21] and offers the ability for simultaneous and selective multi-gas quantification. Almost all gases and volatiles, except the noble gases, can be detected and quantified with only a single measurement[22-24]. As a fast, sensitive and non-consumptive technique, Raman spectroscopy promises a great potential for onsite environmental gas analysis and process monitoring[25, 26].

Materials and Methods

Soil characterization

The sampling of top soil material (0 - 10 cm depth) was conducted in May 2014 from a grassland plot close to Kammerforst, Hainich-Dün region in the western part of the federal state of Thuringia, central Germany. The climate exhibited an annual precipitation of 750-800 mm and an annual average air temperature of 6.8°C (44.2°F). The bedrock consists of Triassic shell limestone covered by a Pleistone loess layer of variable thickness forming soils classified as Stagnosols and Luvisols[27].

For the determination of the organic carbon (C_{org}) and total nitrogen (TN) content and the soil pH, the air dried samples were sieved to < 2 mm. Soil pH was measured in the supernatant of a 1:2.5 mixture of soil and deionized water using a glass electrode (WTW Multi 340i with SenTix41-3 electrode, Weilheim). Oven-dried subsamples for the elemental analysis were homogenized, ground and passed through a 40 µm sieve. Total carbon and nitrogen concentrations were determined by thermal oxidation (Trumac Elementaranalyzer, Leco). After removal of inorganic carbon by repeated washing with 10% hydrogen chloride (HCl), organic carbon was quantified with the same elemental analyzer. The soil texture was determined by laser diffraction particle size analysis (Laser Diffraction Particle Size Analyzer, Beckman Coulter). Table 1 summarizes the soil parameters.

Soil texture			pH (H_2O)	C_{org}	TN	C/N
Clay (%)	Silt (%)	Sand (%)		%	%	
18.1	81.3	0.6	4.87	2.35	0.221	10.65

Table 1: Soil parameters. The top soil was sampled from a grassland plot in the Hainich-Dün region, Thuringia, Germany.

Gas analysis

An innovative Raman gas sensor[28, 29] was applied and adapted for the here reported gas measurements. It is based on a miniaturized laser diode ($\lambda_{excitation}$ = 650 nm, 50 mW), which is frequency locked and feedback-coupled to a power buildup cavity[30] to achieve a power enhancement of 5 orders of magnitude. This enhancement enables monitoring of gas concentrations down to approximately 50 ppm within one second. For a direct quantification of the different gas compounds in a multi-gas mixture pressure, temperature and laser intensity were monitored by additional sensors. The setup was calibrated with the relevant gases, namely nitrogen N_2, oxygen O_2, ^{13}C-labeled benzene $^{13}C_6H_6$, and the carbon dioxide isotopes $^{12}CO_2$ and $^{13}CO_2$. Here, pure $^{13}C_6H_6$ was cooled to 7°C during the calibration to reduce its vapor pressure. By using the Clausius-Clapeyron relation within the ideal gas approximation at low temperatures

$$\ln\frac{p_2}{p_1} = \frac{L}{R}\left(\frac{1}{T_1} - \frac{1}{T_2}\right) , \quad (1)$$

the gaseous benzene concentration could be directly linked to the Raman signal intensity and hence be calibrated. Here, the two sets p_1, T_1 and p_2, T_2 define the thermodynamic states 1 and 2 by their pressure and temperature, respectively. R is the universal gas constant and L the enthalpy of vaporization, which was assumed to be constant. A least square fit of the experimental multi-gas spectrum was performed with the complete so calibrated individual reference spectra in the wavenumber range from 500 to 3000 cm^{-1}. This fitting procedure reveals the concentrations of the particular gas components and is more precise than integrating only the specific peak areas. Additionally, temperature induced wavenumber shifts were precisely corrected by a custom-made software routine.

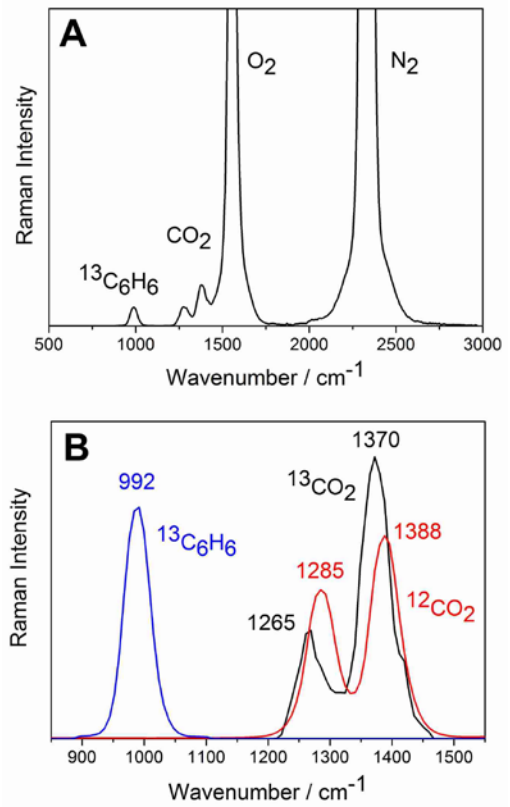

Figure 1: (A) Example of an experimental multi-gas Raman spectrum ($\lambda_{excitation}$ = 650 nm) during the natural attenuation experiment. Most prominent are the rotation-vibrational bands of N_2 (2331 cm^{-1}) and O_2 (1556 cm^{-1}), both with unresolved O and S branches. The concentrations of the individual components were calculated by least-square fitting the multi-gas spectrum with the particular calibration spectra. **(B)** Due to their deviance in the Fermi dyad, the two carbon dioxide isotopes $^{12}CO_2$ (red) and $^{13}CO_2$

(black) can be distinguished. Also depicted is the $^{13}C_6H_6$ mode at 992 cm^{-1} (blue).

Any difference between the measured spectrum and the convoluted calibration spectra also unveils the presence of unexpected, not calibrated gases. These can be added by calibration measurements, which impressively illustrates the versatility of the setup to address not only predetermined gases. All above-mentioned gases can be distinguished without cross-sensitivity by their individual spectral shifts in the acquired Raman spectrum; an exemplary multi-gas spectrum is depicted in Figure 1A. The two carbon dioxide isotopes, $^{12}CO_2$ and $^{13}CO_2$, can be distinguished and simultaneously be quantified due to their deviance in the Fermi dyad (Fig. 1B). The calibration data sets were proven in test measurements with defined gas compositions by mixing of the gas ratios with mass flow controllers. The obtained gas concentrations were normalized for a constant sum of all gas concentrations.

Experimental design

The field-fresh soil was acclimatized to 21°C in a climate chamber one day before beginning the experiment. 200 g were filled in a custom-built Plexiglas column (V = 295 cm^3) and sealed airtight with a screw-in lid enclosing a septum (Fig. 2). In order to establish a reproducible gas composition, the soil headspace (V = 98 cm^3) was flushed with synthetic air (20% O_2, 80% N_2, Linde, Germany), precisely controlled by a mass flow controller (MFC, Brooks Instrument, Germany). During flushing, the gases were quantified and left as exhaust. After a selected time of 150 seconds, the magnetic valves (MV) were switched and closed the inner circuit with the soil column and the Raman gas sensor. A custom-made LabView routine was used for automatic operation of the MV's, the MFC's, and the Raman gas spectrometer. The current headspace gas composition was permanently monitored by the Raman gas sensor. Due to the aerobic soil respiration (here carbohydrate model)

$$C_6H_{12}O_6 + 6\,O_2 \rightarrow 6\,CO_2 + 6\,H_2O \quad , \qquad (2)$$

the $^{12}CO_2$ concentration in the headspace increased with time.

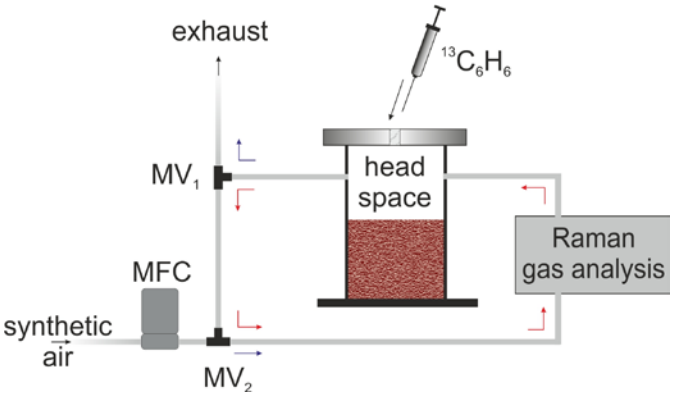

Figure 2: Schematic diagram of the experimental setup. Gas flow during rate measurement and flushing indicated by red and blue arrows, respectively. All gas rates were determined within the closable inner cycle, comprising the soil column and the Raman gas sensor. Using a syringe, the soil was spiked nonrecurring with ^{13}C-labeled benzene and the gas exchange was monitored afterwards.

To avoid any inhibition of this natural process, for instance by back-diffusion into the soil, the $^{12}CO_2$ concentration had to be kept within an environmentally adequate concentration window. Therefore, by reaching a preset $^{12}CO_2$ concentration threshold of 600 ppm, the magnetic valves were switched automatically back to their former state for 150 seconds (feedback control), such that the headspace was flushed with synthetic air again. This eventually reduced the $^{12}CO_2$ concentration in the headspace to approximately 100 ppm and the gas dynamics could be monitored once more afterwards. Using the slope of a linear regression of an individual gas concentration with respect to the time, the respective gas exchange rates could be determined (Figure 3). Here, each fit was only applied for the first 30 minutes of a period between two flushing events in order to stay within the linear flux regime[31]. The rates were normalized by the column surface area of 19.6 cm^2. The microbial respiratory behavior and the natural attenuation characteristics were confirmed in a follow-up experiment under the same conditions (data not shown).

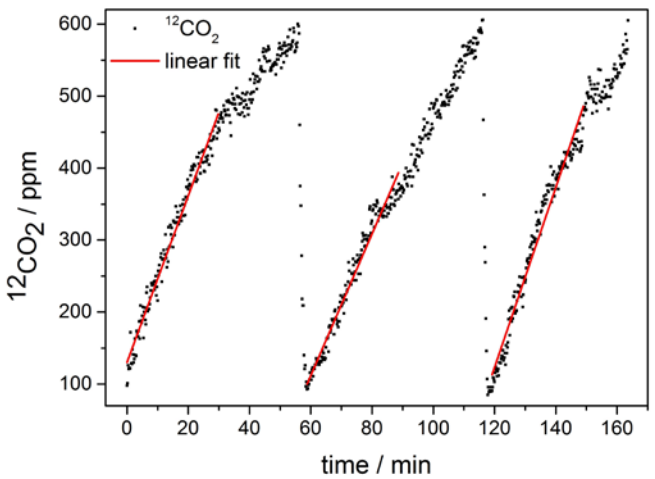

Figure 3: Exemplary quantification of the $^{12}CO_2$ production rates. The change in concentration (black) with respect to time is linearly fitted (red). The linear regression is limited to the first 30 minutes of each cycle to stay within the linear regime. The slope then yields the respective $^{12}CO_2$ gas exchange rate. Other gas rates were calculated accordingly. For better visualization, the time scale in this plot starts at zero-time, which does not match the experimental time scale in this case.

Results and discussion

Gas exchange rates

As mentioned above, the gas exchange rates of the bare, undisturbed soil were analyzed at first (indicated as negative time values in Figure 4). The mean $^{12}CO_2$ concentration rate was 0.72 (± 0.01) µmol m^{-2} s^{-1}, while the mean O_2 concentration rate amounted to -0.74 (± 0.02) µmol m^{-2} s^{-1}. The respiratory quotient (RQ), defined as

the molar ratio of produced units CO_2 per consumed units O_2, yielded 0.98 (± 0.03) on average. This mirrors the case of aerobic soil respiration[32], where the CO_2 evolution and the O_2 uptake are equimolar (Eqn. 2). After measuring several gas exchange rates of the bare soil, the center of the soil surface was spiked with 0.1 ml pure labeled benzene $^{13}C_6H_6$ (Sigma-Aldrich, Germany) using a syringe penetrating the septum (Fig. 2). The syringe was immediately removed after the injection and the septum additionally sealed. Directly after surface spiking, exponential benzene diffusion in the gas phase was observed, different to other models assuming subsurface contaminant injection[33]. Thus, the first post-spiking rates of CO_2 and O_2 in the gas phase were determined 30 minutes after spiking, such that abrupt non-equilibrium diffusion processes did not interfere with these acquired rates. Benzene was oxidized by the soil microorganisms to carbon dioxide and water via[34]

$$C_6H_6 + 7.5\,O_2 \rightarrow 6\,CO_2 + 3\,H_2O \quad . \qquad (3)$$

Hence, for each mol of degraded benzene $^{13}C_6H_6$, 6 mol of $^{13}CO_2$ were produced. This enabled the calculation of the total amount of degraded benzene by measuring the headspace $^{13}CO_2$ concentration. Directly after the injection of benzene at time zero, a huge microbial response became apparent (Figure 4). The $^{12}CO_2$ and O_2 concentration rates were remarkably increased, up to 1.79 and -3.89 µmol m^{-2} s^{-1}, respectively. This strong response in microbial respiration is assumed to result from a phenomenon known as the "Birch effect"[35, 36] describing a rapid release of carbon dioxide from re-wetted soil material. The spiking resulted in an RQ of 0.46, which corresponds to reported RQ values of about 0.4 after the addition of hexadecane to agricultural and forest soils[37]. On the one hand this might be due to the metabolization of those deceased microorganisms[38], which have been most directly exposed to the spiked benzene (caused by heterotrophic microflora); on the other hand from microbial stress demanding more energy for cell repair mechanisms[39]. Within the first hours, the two rates dropped rapidly and the oxygen rate reached a minimum of -0.46 µmol m^{-2} s^{-1} 15 hours after spiking. During this decrease, both gas rates stabilized approximately from 3.5 to 11.5 hours after spiking; the $^{12}CO_2$ rate at 1.1 µmol m^{-2} s^{-1} and the O_2 rate at -2.0 µmol m^{-2} s^{-1}. However, the $^{13}CO_2$ rate remained unaffected within the first 12 hours, indicating that no measurable degradation of the labeled benzene took place. While the $^{12}CO_2$ rate decreased further after 15 hours, the O_2 rate increased again. This contrary behavior coincided with the emergence of the $^{13}CO_2$ production, demonstrating the initiated degradation of the labeled benzene, which accompanies an increased oxygen demand.

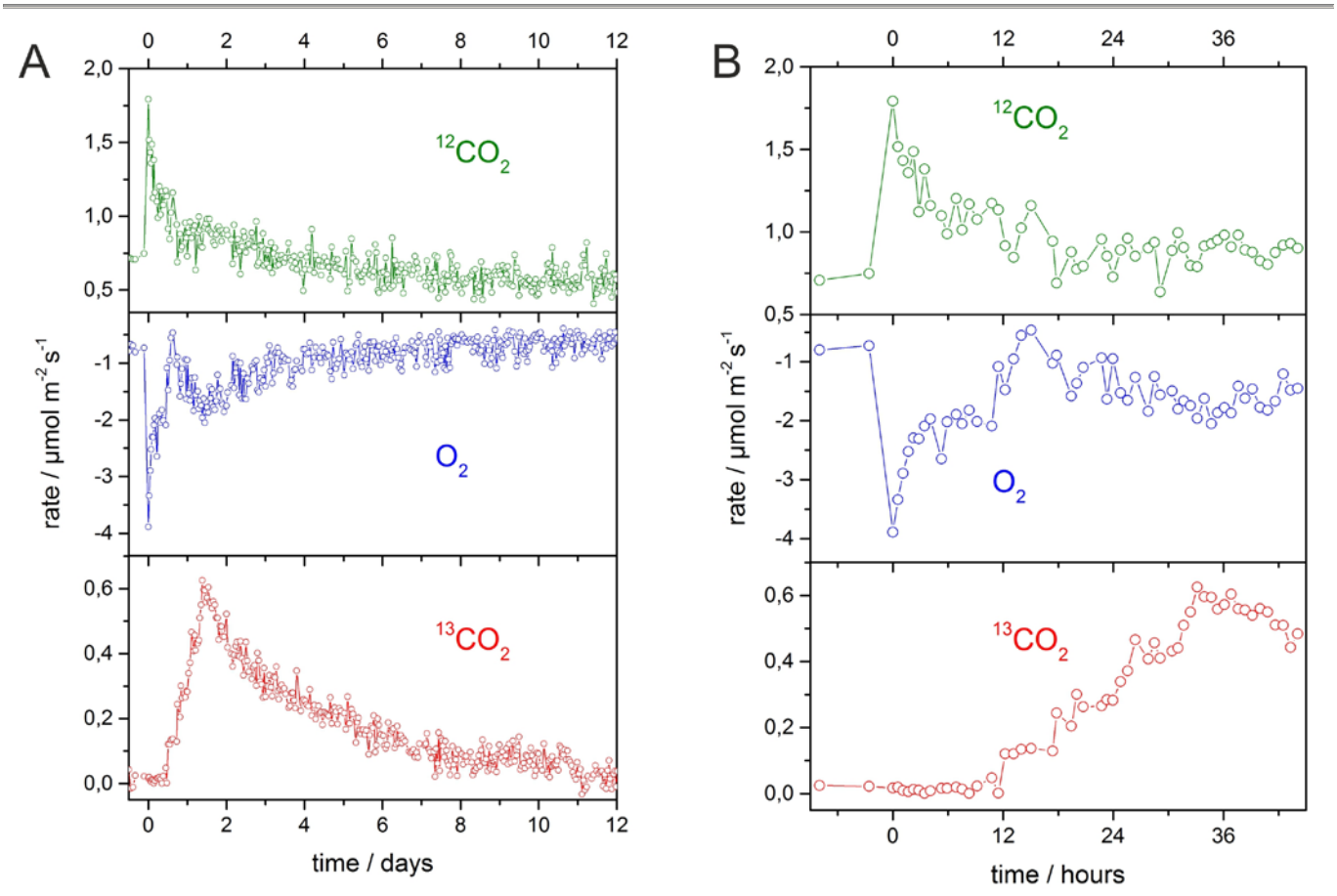

Figure 4: (A) Evolution of the $^{12}CO_2$ (top), O_2 (center) and $^{13}CO_2$ (bottom) rates. Negative times correspond to the pre-spiking phase. **(B)** Detailed view onto the first 45 hours of the experiment after spiking.

The maximum $^{13}CO_2$ rate of 0.63 µmol m^{-2} s^{-1} was reached 33 hours after spiking. This time corresponds with reported time windows after application of D-glucose on soils[40] or benzene to pure cultures isolated from soils[41]. On the other hand, the observed 33 hours until maximum degradation was reached, differ from reported - typically longer - times in cases when benzene[42] or hydrocarbons[43] were thoroughly mixed with the complete soil mass. After 34 hours - about the same time as the $^{13}CO_2$ production rate reached the maximum - the O_2 consumption rate peaked at -2.06 µmol m^{-2} s^{-1}, depicting again the correlation of $^{13}CO_2$ production and O_2 uptake. An RQ of 0.72 was measured at time of highest $^{13}CO_2$ rates 33 hours after spiking, which is in good agreement with the theoretical RQ of 0.8 during benzene degradation, obtained by the stoichiometric Equation 3. The concentrations of all three gas rates - $^{12}CO_2$, O_2 and $^{13}CO_2$ - decreased continuously during the rest of the experiment. The $^{13}CO_2$ production disappeared 12 days after the spiking event. At the end of the experiment, the mean $^{12}CO_2$ rate amounted to 0.58 (± 0.02) µmol m^{-2} s^{-1}, the mean O_2 rate was -0.63 (± 0.03) µmol m^{-2} s^{-1}. These rates were slightly lower than the respective pre-spiking rates. This suggests that the microbes perished partly due to the lethal impact of the benzene, which then resulted in a lowered overall microbial respiratory activity. A mean RQ of 0.96 (± 0.04) was reached 12 days after the spiking event. Thus, the soil returned to the characteristic aerobic respiration following Eqn. 2.

Benzene fate

The benzene diffusion into the atmosphere was further investigated in order to quantify the degradation process. Utilizing the online multi-gas detection ability provided by the CERS sensor, the headspace concentration of the labeled benzene $^{13}C_6H_6$ was continuously monitored and analyzed. Due to its high vapor pressure (approximately 10.4 kPa at 21°C)[44] and the direct surface application by the spiking, most of the benzene evaporated and diffused into the headspace. Diffused benzene was calculated by measuring the difference of initial and final concentration during the flushing events, because of the observed non-linearity of the benzene flux. $^{13}C_6H_6$ diffusion dropped exponentially, which is in good agreement with theoretical calculations[45]. The total amount of diffused benzene is depicted in Figure 5A. After 4 hours already half of the added benzene passed into the gaseous phase. The strong diffusion ended after almost 6.5 days. By then, 1025 µmol $^{13}C_6H_6$ diffused in total, which corresponds to 91.4 % of the spiked mass. The total amount of degraded benzene was calculated by integration of the $^{13}CO_2$ production rates. Because 6 carbon dioxide molecules were produced per consumed benzene molecule, the total amount of degraded $^{13}C_6H_6$ could be directly evaluated (Fig. 5B). After a lag time of 12 hours, $^{13}CO_2$ was monitored in the column headspace, indicating the advent of the degradation process. Approximately 40 µmol $^{13}C_6H_6$ were degraded after 12 days, which was equivalent to 3.6 % of the spiked benzene. Thus, in total 95 % of the added $^{13}C_6H_6$ found their way into the headspace after 12 days, either by diffusion or degraded into $^{13}CO_2$. Several studies on transport and diffusion of organic compounds in unsaturated soil columns[46, 47] suggest that the remainder most likely diffused into subjacent soil layers. Those mechanisms will be studied in more detail (e.g. under varying benzene concentrations and soil pH) in further experiments.

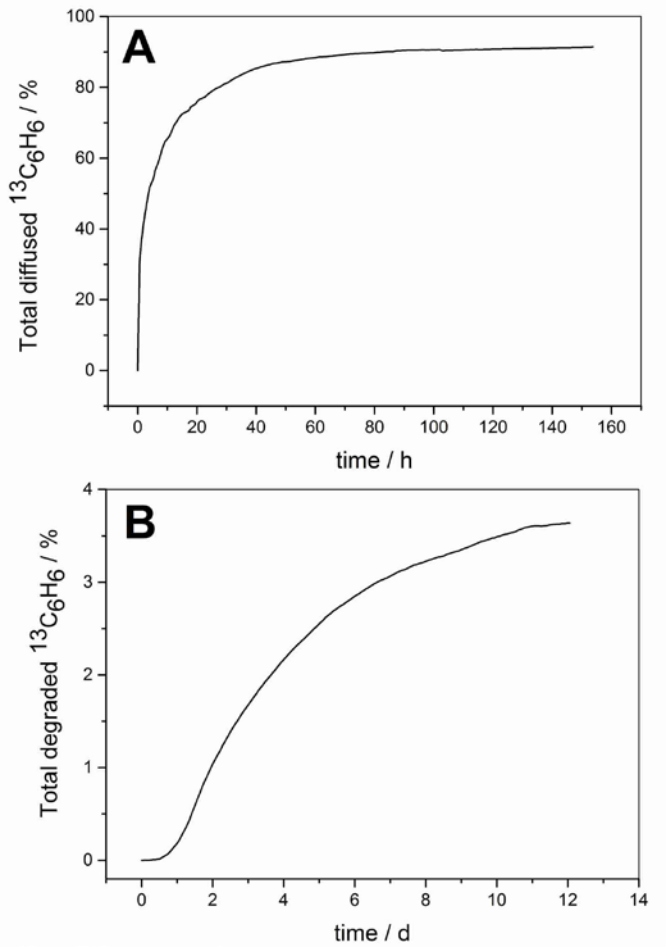

Figure 5: (A) Diffusion of the spiked benzene from the soil surface into the headspace. **(B)** Biodegradation dynamics of benzene. The total amount of degraded benzene was calculated by integration of the $^{13}CO_2$ production rates.

Conclusion

In summary, cavity enhanced Raman gas sensing was demonstrated as a supremely versatile technique for online monitoring of multi-gas compositions consisting of $^{12}CO_2$, $^{13}CO_2$, O_2, and $^{13}C_6H_6$ with just one single measurement. The application of CERS is non-consumptive, such that continuous and quantitative gas measurements are feasible, while preventing manipulations of the gas composition. The high temporal resolution and automated design of the Raman gas setup enabled analyzing rapid gas dynamics and elucidating the accompanied chemical processes behind. In this work, CERS was applied for the quantification of the natural attenuation of ^{13}C-labeled benzene after superficial application on a silty-loamy soil surface, representing sudden contamination events

e.g. at petrol stations or industrial plants. The impact of benzene spiking on the microbial respiratory activity was investigated. The monitored RQ effectively indicated the subsequent microbial phases, from the aerobic pre-spiking respiration (RQ value of almost 1) to the immediate response to the benzene application with low RQ values and an increased oxygen demand; then the maximum degradation phase with a RQ close to theoretical values of 0.72 and eventually the return to the aerobic respiration again. Considering the unique versatility and selectivity of cavity enhanced Raman gas sensing and its high potential for miniaturization, we foresee that new CERS will develop to an important technique for the gas analysis of contaminated soils.

Acknowledgements

The authors kindly acknowledge the support by the Collaborative Research Centre AquaDiva, funded by the German Science Foundation (SFB 1076). We thank Robert Keiner for advice on Raman sensor operation.

Notes and references

[a] Leibniz Institute of Photonic Technology, Jena, Germany
[b] Friedrich Schiller University, Institute of Geography, Jena, Germany
[c] Friedrich Schiller University, Institute for Physical Chemistry, Jena, Germany
[d] Friedrich Schiller University, Abbe Center of Photonics, Jena, Germany
* Corresponding author: torsten.frosch@uni-jena.de, torsten.frosch@gmx.de, phone: +49 3641 206221

1. H. White, ed. U. S. EPA., Washington, DC, 1999.
2. H. Rugner, M. Finkel, A. Kaschl and M. Bittens, *Environmental Science & Policy*, 2006, 9, 568-576.
3. M. Tyagi, M. M. R. da Fonseca and C. C. C. R. de Carvalho, *Biodegradation*, 2011, 22, 231-241.
4. M. Megharaj, B. Ramakrishnan, K. Venkateswarlu, N. Sethunathan and R. Naidu, *Environment International*, 2011, 37, 1362-1375.
5. C. N. Mulligan and R. N. Yong, *Environment International*, 2004, 30, 587-601.
6. E. Jindrova, M. Chocova, K. Demnerova and V. Brenner, *Folia Microbiologica*, 2002, 47, 83-93.
7. B. Michalzik and B. Stadler, *Basic and Applied Ecology*, 2000, 1, 117-123.
8. J. F. Pankow, W. Luo, A. N. Melnychenko, K. C. Barsanti, L. M. Isabelle, C. Chen, A. B. Guenther and T. N. Rosenstiel, *Atmospheric Measurement Techniques*, 2012, 5, 345-361.
9. M. Deppe, K. H. Knorr, D. M. McKnight and C. Blodau, *Biogeochemistry*, 2010, 100, 89-103.
10. O. Heinemeyer, H. Insam, E. A. Kaiser and G. Walenzik, *Plant and Soil*, 1989, 116, 191-195.
11. J. Iqbal, M. J. Castellano and T. B. Parkin, *Global Change Biology*, 2013, 19, 327-336.
12. S. Hashimoto, *Soil Biology & Biochemistry*, 2002, 34, 273-275.
13. E. R. Crosson, *Applied Physics B-Lasers and Optics*, 2008, 92, 403-408.
14. A. J. Rixon and B. J. Bridge, *Nature*, 1968, 218, 961-&.
15. R. A. Halvorson and P. J. Vikesland, *Environmental Science & Technology*, 2010, 44, 7749-7755.
16. T. Frosch, D. Yan and J. Popp, *Analytical Chemistry*, 2013, 85, 6264-6271.
17. T. Frosch, S. Koncarevic, L. Zedler, M. Schmitt, K. Schenzel, K. Becker and J. Popp, *J. Phys. Chem. B*, 2007, 111, 11047-11056.
18. T. Frosch, T. Meyer, M. Schmitt and J. Popp, *Analytical Chemistry*, 2007, 79, 6159-6166.
19. P. J. Hendra and C. J. Vear, *Analyst*, 1970, 95, 321-342.
20. T. Frosch and J. Popp, *Journal of Molecular Structure*, 2009, 924-926, 301-308.
21. T. Frosch, S. Koncarevic, K. Becker and J. Popp, *Analyst*, 2009, 134, 1126-1132.
22. R. Keiner, T. Frosch, S. Hanf, A. Rusznyak, D. M. Akob, K. Kusel and J. Popp, *Analytical Chemistry*, 2013, 85, 8708-8714.
23. S. Hanf, T. Bögözi, R. Keiner, T. Frosch and J. Popp, *Analytical Chemistry*, 2015, 87 (2), 982-988.
24. T. Bögözi, J. Popp and T. Frosch, *Bioanalysis* 2015, 7 (3), 281–284.
25. R. Keiner, M. C. Gruselle, B. Michalzik, J. Popp and T. Frosch, *Analytical and Bioanalytical Chemistry* 2015, DOI: 10.1007/s00216-014-8446-8.
26. S. Hanf, R. Keiner, D. Yan, J. Popp and T. Frosch, *Analytical Chemistry*, 2014, 86, 5278-5285.
27. IUSS Working Group WRB, in *World Soil Resources Reports No. 103*, FAO Rome, 2006.
28. R. Keiner, T. Frosch, T. Massad, S. Trumbore and J. Popp, *Analyst*, 2014, 139, 16, 3879-3884.
29. T. Frosch, R. Keiner, B. Michalzik, B. Fischer and J. Popp, *Analytical Chemistry* 2013, 85, 1295-1299.
30. D. A. King and R. J. Pittaro, *Optics Letters*, 1998, 23, 774-776.
31. T. Naganawa and K. Kyuma, *Soil Science and Plant Nutrition*, 1991, 37, 381-386.
32. F. Mavituna and B. Atkinson, *Biochemical engineering and biotechnology handbook*, Nature Press, New York, N.Y., 1983.
33. P. Du, M. Sagehashi, A. Terada, S. Zhou, F. S. Li and M. Hosomi, *Soil Science Society of America Journal*, 2011, 75, 2147-2157.
34. T. H. Wiedemeier, J. T. Wilson, D. H. Kampbell, R. N. Miller and J. E. Hansen, *Technical Protocol for Implementing Intrinsic Remediation with Long-Term Monitoring for Natural Attenuation of Fuel Contamination Dissolved in Groundwater. Volume II*, DTIC Document, 1995.
35. H. F. Birch, *Nature (London, U. K.)*, 1958, 182, 1172.
36. H. F. Birch, *Plant and Soil* 1959, IX, 262-286.
37. O. Dilly, S. Nii-Annang, G. Franke, T. Fischer, F. Buegger and A. Zyakun, *Soil Biology & Biochemistry*, 2011, 43, 1808-1811.
38. E. A. Steinhaus and J. M. Birkeland, *Journal of Bacteriology*, 1939, 38, 249-261.
39. F. Scheffer and P. Schachtschabel, *Lehrbuch der Bodenkunde*, Spektrum Akademischer Verlag, Heidelberg, 2010.
40. R. W. O'Dowd and D. W. Hopkins, *Soil Biology & Biochemistry*, 1998, 30, 2009-2016.
41. K. Haider, G. Jagnow, R. Kohnen and S. U. Lim, *Archives of Microbiology*, 1974, 96, 183-200.
42. W. X. Zhang and E. J. Bouwer, *Biodegradation*, 1997, 8, 167-175.
43. E. Lamy, T. C. Tran, S. Mottelet, A. Pauss and O. Schoefs, *International Biodeterioration & Biodegradation*, 2013, 83, 85-91.
44. P. D. Golding and W. D. Machin, *Journal of the Chemical Society-Faraday Transactions I*, 1987, 83, 2719-2726.
45. D. R. Shonnard and R. L. Bell, *Environmental Science & Technology*, 1993, 27, 2909-2913.
46. E. A. Voudrias and C. Y. Li, *Journal of Hazardous Materials*, 1993, 34, 295-311.
47. R. Arands, T. Lam, I. Massry, D. H. Berler, F. J. Muzzio and D. S. Kosson, *Water Resources Research*, 1997, 33, 599-609.

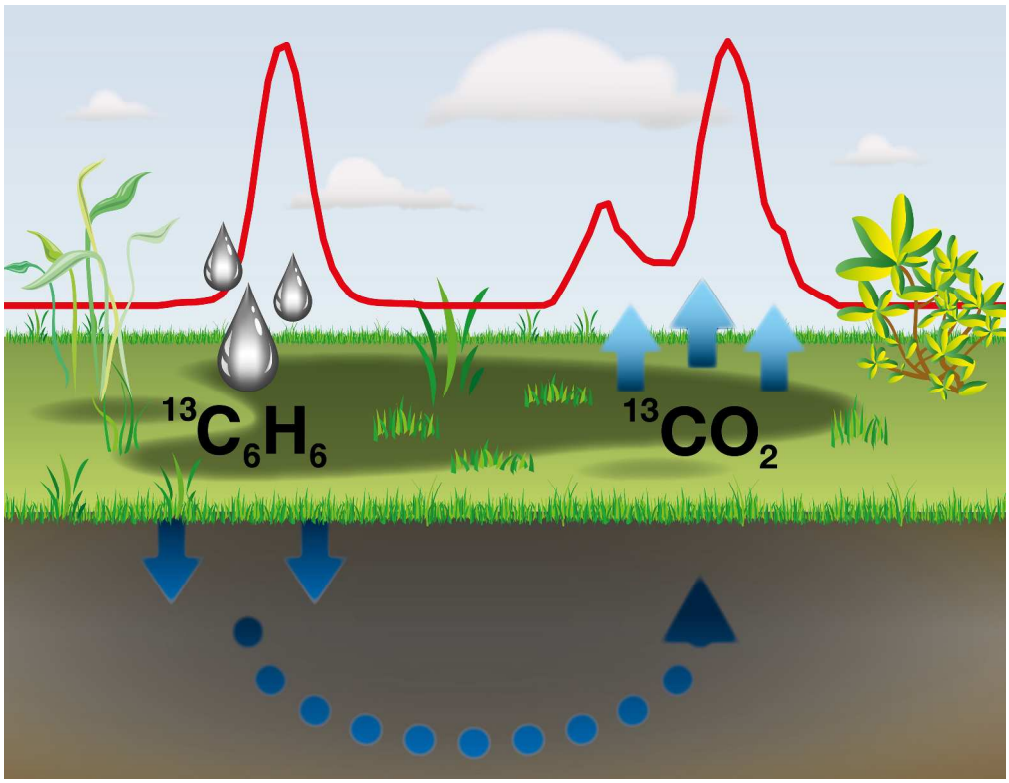

Cavity enhanced Raman multi-gas spectroscopy was proven as beneficial technique for rapid onsite monitoring of contaminant bioremediation and microbial activity.
1749x1352mm (72 x 72 DPI)